Scripta Materialia 140 (2017) 59–62

Contents lists available at ScienceDirect

Scripta Materialia

journal homepage: www.elsevier.com/locate/scriptamat

Regular Article

Laves phase intermetallic matrix composite in situ toughened by ductile precipitates

Alexander J Knowles[a, b,*], Ayan Bhowmik[b], Surajit Purkayastha[a], Nicholas G Jones[a], Finn Giuliani[b], William J Clegg[a], David Dye[b], Howard J Stone[a]

[a] Department of Materials Science and Metallurgy, University of Cambridge, Cambridge CB3 0F3, UK
[b] Department of Materials, Imperial College, South Kensington, London SW7 2AZ, UK

ARTICLE INFO

Article history:
Received 8 June 2017
Received in revised form 22 June 2017
Accepted 23 June 2017
Available online xxxx

Keywords:
Intermetallics
Composites
Precipitation
Orientation relationship
Mechanical properties

ABSTRACT

Laves phase based materials are of interest for elevated temperature applications for their high melting points and strengths but are critically limited by their low fracture toughness. Here, a Laves phase intermetallic matrix composite toughened by ductile precipitates has been studied. This microstructure was produced in situ by heat treating a Fe_2(Mo,Ti) based alloy to precipitate ~12% volume fraction of fine ~250 nm bcc, A2 (Mo,Ti), phase, with an orientation relationship of $[100]_{C14}//[113]_{A2}$, $[010]_{C14}//[1\bar{1}\bar{1}]_{A2}$, $[001]_{C14}//[12\bar{1}]_{A2}$. The precipitated A2 phase increased the indentation fracture toughness from 1.1 to 2.2 MPa $m^{1/2}$ while maintaining a high hardness of $HV_{0.5}$ = 8.9 GPa similar to monolithic Laves phases.

The high melting points and strengths of Laves phases are attractive for elevated temperature structural materials [1–3]. A particular focus has been the *ABC* series of Laves phases, where *A* and *B* are transition metals, such as iron, titanium and/or refractory metals, while *C* is a ternary addition of Al or Si, in order to confer oxidation resistance [4]. However, as with many intermetallics, their fracture toughnesses are low, typically ~1 MPa $m^{1/2}$ [3,5,6]. Microstructural modifications and alloying strategies are therefore required to increase the toughness of Laves phase based materials to produce engineering-relevant materials.

In this study, an alloy based on the C14 Fe_2Ti Laves phase was studied. Such Laves phase alloys have been demonstrated to exhibit high microhardness of ~10 GPa [7]. Furthermore, the Fe_2Ti Laves phase has been shown to be able to accommodate up to 33 at.% Al [8], offering the prospect of alloying for oxidation resistance. Alloying with a refractory metal is of interest because of their high melting points and low diffusivities [6]. Mo substitutes on the Ti site following the formula Fe_2(Ti, Mo) [9,10] and Mo additions have been shown to result in an increase in hardness [7]. Further, it has been shown that the off-stoichiometric solubility for Ti and Mo within Fe_2(Ti, Mo) decreases with temperature [9]. Owing to this change in solubility with temperature, fine A2 (Mo, Ti) precipitates may be formed within a C14 Fe_2(Ti, Mo) matrix offering the potential of ductile phase toughening while maintaining the strength of the majority Laves phase. In this study a Fe-30Ti-10Mo (at.%) alloy was selected to explore the toughening effect of A2 (Mo, Ti) precipitates within a Laves phase intermetallic matrix composite and their influence on hardness.

The alloy was vacuum arc melted from pure elements (>99.9%) and remelted five times, with inter-melt flipping to improve homogeneity. A section of the alloy was encapsulated in an argon backfilled quartz ampoule, aged at 1000 °C for 500 h and water quenched, after [9].

The alloy was evaluated in both the as-cast and aged conditions by scanning electron microscopy (SEM). Energy dispersive X-ray spectroscopy (EDX) at 20 kV was used to assess the bulk alloy composition by performing 200 × 400 μm area scans across the ingot, while point measurements were used to assess individual phases, with a probe diameter estimated to be ~1 μm. Foils for transmission electron microscopy (TEM) and scanning TEM (STEM) were produced by electro-polishing using a solution of 10 vol.% perchloric acid in methanol at −30°C and 18 V, followed by ion polishing. X-ray diffraction (XRD) data were collected on a Cu source diffractometer and were fitted using the Pawley method in the TOPAS software package.

* Corresponding author at: Department of Materials Science and Metallurgy, University of Cambridge, Cambridge CB3 0F3, UK.
E-mail address: a.knowles@ic.ac.uk (A.J. Knowles).

http://dx.doi.org/10.1016/j.scriptamat.2017.06.043
1359-6462/

The mechanical properties of the alloy were evaluated in the aged condition. Microhardness measurements were performed using loads of 100 g ($HV_{0.1}$) or 500 ($HV_{0.5}$) held for 10 s, with the corner crack length measured using SEM. Nanoindentation testing was performed with a Berkovich indenter tip to produce thirty 400 nm deep indents giving hardness and modulus measurements, in addition to twenty 1500 nm deep indents, which had corner cracks that were used to probe the local toughness. Each indent was examined by SEM and binned with respect to the area fraction of second phase present in the ~5 μm diameter local region to 0–5, 5–10 or 10–30%, corresponding to the prior dendrite cores, dendrite peripheries and interdendritic regions.

The bulk composition was determined by area EDX to be (59.8 ± 0.1)Fe–(29.7 ± 0.2)Ti–(10.5 ± 0.2)Mo (average ± standard deviation in at.%), which was close to the target composition, while the low standard deviation indicated that there was minimal macrosegregation present. In the as-cast condition backscattered electron (BSE) imaging identified a two-phase microstructure with dark contrast dendrites along with a brighter interdendritic phase of higher average Z, Fig. 1a. The dendrite arm spacing calculated by the mean linear intercept method was ~40 μm [11]. The as-cast XRD pattern contained strong C14 reflections, along with minor $D8_5$ reflections, Fig. 1e. Since the sample was not in a powdered state it was not possible to perform a Rietveld refinement. Pawley refinement found the C14 phase lattice parameters to be $a = 4.83 \pm 0.01$ Å and $c = 7.87 \pm 0.01$ Å, while those of the $D8_5$ phase were $a = 4.84 \pm 0.01$ Å and $c = 26.0 \pm 0.01$ Å. SEM-EDX found the dendrites to have a composition of (61.23±0.47)Fe–(29.82±0.36)Ti–(8.96±0.11)Mo, consistent with them being C14 Fe_2(Ti, Mo). In addition, the dendrites were found to be cored, with the centres ~0.5%Mo richer than the peripheries. The interdendritic regions were found to have a composition of (53.2 ± 0.16)Fe–(27.87 ± 0.37)Ti–(18.94 ± 0.53)Mo, which was consistent with those reported for $D8_5$ Fe_7(Mo, Ti)$_6$ [10,13].

Following heat treatment of the alloy at 1000 °C for 500 h, fine bright laths 250 ± 100 nm wide and 2.5 ± 2 μm long were found to have precipitated within the C14 dendrites, Fig. 1b and c. The dendrite cores had 0–5% area fraction of laths, while the dendrite peripheries had a higher area fraction of 5–10% of the bright phase, which were confirmed to be laths rather than needles by focussed ion beam serial sectioning (see Fig. 1 in [12]). In addition, the $D8_5$ interdendritic regions present in the as-cast condition (Fig. 1a) were instead found to contain an interpenetrating network of majority dark phase with 10–30% area fraction bright phase, with a separation of 250 ± 250 nm, Fig. 1d. The fine scale of the phases throughout the alloy after aging at 1000 °C for 500 h indicated that the microstructure was resistant against coarsening, which was attributed to the slow diffusion rate of Mo within the C14 Laves phase matrix. The XRD pattern collected from the heat treated alloy contained strong C14 reflections, with $a = 4.81 \pm 0.01$ Å and $c = 7.91 \pm 0.01$ Å, Fig. 1e [9]. However, no $D8_5$ reflections were identified, with the additional reflections observed instead being from an A2 phase, $a = 3.13 \pm 0.01$ Å. The composition of the phases were determined in a previous study, with the C14 matrix found to be (63.4±0.3)Fe–(31.4±0.2)Ti–(5.2 ± 0.4)Mo using SEM-EDX, and (66.3 ± 0.4)Fe–(29.3 ± 0.7)Ti–(4.4 ± 1.0)Mo using TEM-EDX [9]. While the bright phase was too fine to be analysed by SEM-EDX, it was determined by TEM-EDX to be (3.9 ± 0.6)Fe–(15.2 ± 0.9)Ti–(81.0 ± 1.4)Mo, which was consistent with A2 (Mo, Ti) [9]. This supported STEM-EDX mapping that found Mo to be rejected from the C14 matrix into the A2 precipitates (see Fig. 2 in [12]). The phases identified in the as-cast and aged alloy were consistent with the Fe-Mo-Ti ternary phase diagram [9,10,13]. The lever rule calculated molar percent of A2 phase was 9%, using the measured bulk and phase compositions, which was in good agreement with the 12% average area percent A2 observed in BSE micrographs (Fig. 1b–d). Owing to the ~0.5%Mo coring present in the as-cast condition, the area fraction of A2 (Mo, Ti) precipitates was higher at the C14 Fe_2(Ti, Mo) dendrite peripheries than their cores (Fig. 1b). Simultaneously, the prior interdendritic $D8_5$ phase regions underwent a eutectoid decomposition into C14 Fe_2(Ti, Mo) and A2 (Mo, Ti) during the 1000 °C heat treatment (Fig. 1d), this is consistent with the reported decrease in the off-stoichiometric solubility for Mo and Ti within Fe_7(Mo, Ti)$_6$ with temperature [9,13].

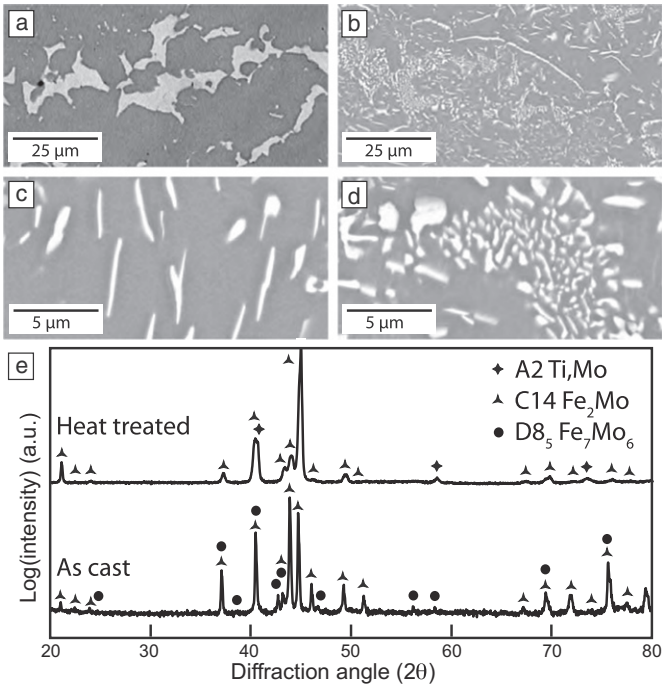

Fig. 1. BSE SEM micrographs of the alloy in (a) the as-cast condition, (b) heat treated at 1000 °C with detailed views of (c) a prior dendritic region and (d) a prior interdendritic region. (e) XRD patterns collected in each condition.

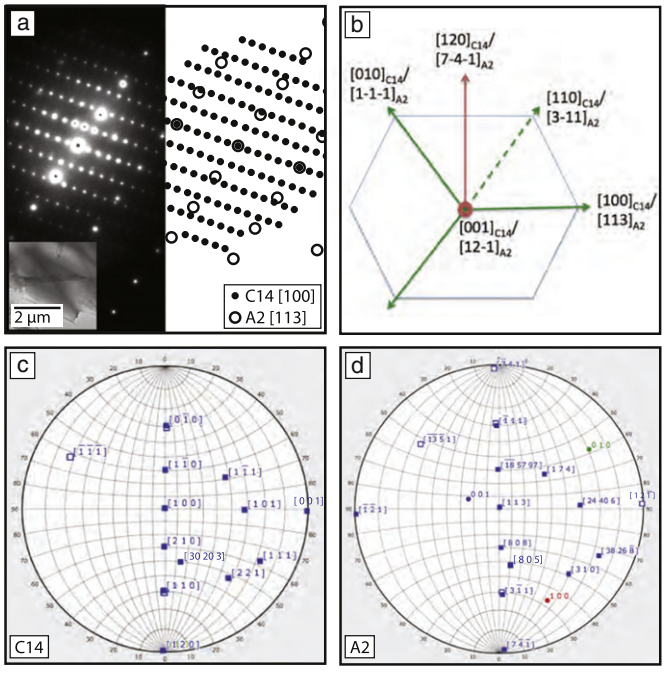

Fig. 2. Heat treated alloy (a) SAPD and key of $[100]_{C14}$ $[113]_{A2}$ with brightfield micrograph inset, (b) schematic of the basal C14 and corresponding $\{12\bar{1}\}$ A2 plane overlap, as well as (c) $[100]_{C14}$ and (d) $[113]_{A2}$ stereographic projections.